arXiv:1601.06337v1 [gr-qc] 24 Jan 2016

The Geometrical Structure of the Tolman VII solution

Ambrish M. Raghoonundun

David W. Hobill

Abstract. The Tolman VII solution, an exact analytic solution to the spherically symmetric, static Einstein equations with a perfect fluid source, has many characteristics that make it interesting for modelling high density physical astronomical objects. Here we supplement those characteristics with the geometrical tensors that this solution possess, and find that the Weyl, Riemann, and Ricci tensor components show unexpected mathematical behaviour that change depending on physically motivated parameters, even though the mass of the modelled objects is fixed. We show these features firstly through tensor components, and then through the scalars in the null tetrad formalism of Newmann and Penrose. The salient conclusion of this analysis is the intimate relationship between the Tolman VII solution and the constant density Schwarzschild interior solution: the former being a straight forward generalization of the latter while eschewing the unphysical constant density.

PACS numbers: 04.40.Dg, 04.20.Jb ,02.40.-k

1. Introduction

The Tolman–Oppenheimer–Volkoff (TOV) equation is commonly used to construct static spherically symmetric solutions of self-gravitating objects consistent with general relativity. The TOV equation is particularly useful for studies of white dwarfs, neutron stars, and quark stars. This equation can be seen as a generalization of the Lane-Emden equation of Newtonian stars to general relativistic ones. If the aim of the study is the prediction of masses and radii of compact objects this is where the analysis usually terminates, since this type of analysis is used to constrain equations of state (EOS) of matter in the high density regimes. The usual view is that since the TOV equation is derived from general relativistic considerations, a proper general relativistic model incorporating all of known physics has been found. In this article the goal is to show that even if one is given an EOS, a host of other geometrical properties that are not readily apparent can also be obtained. What will allow such an analysis is the availability of an exact closed form solution that also yields a physical EOS. By inverting the flow of the historical derivation of this solution, one can show how starting with an EOS that is well behaved, geometrical tensors can be generated. The geometrical information presented here will be in the Riemann and Weyl tensors and in the Ricci tensor and scalar. Together with the metric these provide a complete geometrical description of the behaviour of the solution, and since the solution being discussed is physical [1, 2], the description is hopefully applicable to the real world.

The point of view to be pursued in this article is that the exterior vacuum geometry is described by the Schwarzschild exterior metric due to some central object whose interior consists of a perfect fluid. The exterior field is determined solely by the Schwarzschild mass seen outside, but what will be shown here is that even with a unique interior solution modulo parameters, the behaviour, and qualities of the material inside can be very different. The geometrical tensors are found to be parameter dependent, and indeed one expects the Ricci tensor R_{ab} components, and the Ricci scalar R, to change with the interior solution parameters. That the Weyl tensor C_{abcd} components which usually encode the free gravitational field has a different behaviour depending on these parameters is perhaps surprising.

This article is organized as follows: following a brief description of the solution in section 2, a brief review of the different definitions of mass in general relativity is given in section 3. The fixing of certain parameters is thus achieved through these definitions before continuing with a thorough geometrical analysis of the solution. The behaviour of the metric and other tensors is discussed in section 4. Then two different tetrads are introduced: an orthogonal one in section 5.1 and a null one in section 5.2, to express the tensor quantities found previously in the different tetrad bases, before discussing the results in section 6. Finally a set of expressions and graphs of the tetrad formalism quantities is provided in the appendix

2. The Tolman VII solution

The Tolman VII solution was generated through a mathematical ansatz on the static, spherically symmetric Einstein's equations by Tolman [3] in 1939. Several authors [4, 5] subsequently proved that it was a viable *physical* solution, and showed [2] that it could be used advantageously to model compact astrophysical objects. An interesting aspect of the Tolman VII solution is that an exact analytic equation of state can be obtained for it. Since a closed form solution exists, all geometrical quantities of interest can be computed directly. The behaviour of these we claim gives insight into exactly which parts of the external field is influenced by which internal contributions. In particular it is found that the Weyl tensor contribution in the interior is only sometimes continuous with the pure Weyl Schwarzschild exterior, and that the Ricci tensor components which is always zero outside the star, has interesting non-monotonic behaviour inside the star, pointing towards non-intuitive curvature behaviour in the interior of stars.

The Tolman VII solution is completely specified by the two metric functions $Z(r) = \mathrm{e}^{-\lambda(r)}$ and $Y(r) = \mathrm{e}^{\nu(r)/2}$ of the spherically symmetric and static line element

$$\mathrm{d}s^2 = \mathrm{e}^{\nu(r)}\mathrm{d}t^2 - \mathrm{e}^{\lambda(r)}\mathrm{d}r^2 - r^2\mathrm{d}\theta^2 - r^2\sin^2\theta\mathrm{d}\varphi^2,$$

a mass density function ρ, and an isotropic pressure p : all of which are functions of r, the Schwarzschild radial coordinate.

A $(+,-,-,-)$ signature is used along with geometrical units where $G = c = 1$. Commencing with a quadratic mass density function of the form

$$\rho(r) = \rho_c\left[1 - \mu\left(\frac{r}{r_b}\right)^2\right], \tag{1}$$

the three constants, ρ_c being the central density at $r = 0$ in the star, while r_b is the coordinate radius of the boundary, and μ is a "self-boundedness" parameter that allows for the surface density to be zero when $\mu = 1$ and non-zero for $0 \leq \mu < 1$, as will become clear in what follows; the Einstein equations lead directly to the first metric function,

$$Z(r) = 1 - \left(\frac{\kappa\rho_c}{3}\right)r^2 + \left(\frac{\kappa\mu\rho_c}{5r_b^2}\right)r^4 =: 1 - br^2 + ar^4. \tag{2}$$

With a little bit more effort (see for example [6, 2]) the second metric function given by

$$Y(r) = c_1\cos(\phi\xi(r)) + c_2\sin(\phi\xi(r)), \quad \text{with } \phi = \sqrt{\frac{a}{4}}. \tag{3}$$

can be obtained, from which simple manipulations of the Einstein equations lead to the very complicated looking expression for the pressure:

$$\kappa p = \frac{4\phi[c_2\cos(\phi\xi) - c_1\sin(\phi\xi)]\sqrt{1 - br^2 + ar^4}}{c_1\cos(\phi\xi) + c_2\sin(\phi\xi)} - 4ar^2 + 2b - \kappa\rho, \tag{4}$$

where the transformed radial coordinate ξ whose expression is

$$\xi(r) = \frac{2}{\sqrt{a}} \coth^{-1}\left(\frac{1+\sqrt{1-br^2+ar^4}}{r^2\sqrt{a}}\right), \tag{5}$$

has been used. The complicated form of this pressure is the reason Tolman initially abandoned [3] this solution, but it was shown previously [2, 7, 8] that this function has some very rich physical properties.

The constants c_1 and c_2 are fully determined through

$$c_1 = \gamma\cos(\phi\xi_b) - \frac{\alpha}{\phi}\sin(\phi\xi_b), \tag{6a}$$

$$c_2 = \gamma\sin(\phi\xi_b) + \frac{\alpha}{\phi}\cos(\phi\xi_b), \tag{6b}$$

once boundary conditions are imposed, where

$$\alpha = \frac{\kappa\rho_c}{4}\left(\frac{1}{3}-\frac{\mu}{5}\right),$$

$$\gamma = \sqrt{1-\kappa\rho_c r_b^2\left(\frac{1}{3}-\frac{\mu}{5}\right)},$$

while a, and b are constants that are defined through equation (2). As for ξ_b, it is a shorthand for the value of the function $\xi(r)$ which was provided in equation (5), evaluated at the boundary, $r = r_b$.

At this juncture, it will be beneficial to note that this form for the Z metric function can be seen as a generalization of the Schwarzschild interior solution: indeed, were one to only use the first two terms in the expression of Z, the end result would be the exact form of the Schwarzschild interior solution's Z function: this parallel between Tolman VII and Schwarzschild interior will become clearer in this article. This generalization relation has been erroneously interpreted previously in [9], where it was stated that the limit of the equivalent of $\mu = 0$ does not yield the Schwarzschild interior solution. The is untrue, but the issue relates to how the differential equation for Y is solved. The final form of the equation to be solved is a harmonic oscillator type equation whose solutions for zero frequency corresponds to the Schwarzschild interior solution when $\mu = 0$. The Tolman VII solution by contrast corresponds to positive frequency trigonometric solutions whose limit when $\mu \to 0$, does not give the linear solution as the frequency goes to zero. The similarity to the Schwarzschild interior solution is also evident in the equation for the density (1) in the limit of $\mu = 0$ when one gets the constant density solution – a well know characteristic of Schwarzschild interior.

Since the vacuum region is spherically symmetric and static, the only candidate by Birkhoff's theorem is the Schwarzschild exterior solution. The Israel-Darmois junction conditions for this system can then be shown to be equivalent to the following two conditions [10]:

$$p(r_b) = 0, \quad \text{and}, \tag{7a}$$

$$Z(r_b) = 1 - \frac{2M}{r_b} = Y^2(r_b). \tag{7b}$$

Where $M = m(r_b)$ is the total mass of the sphere as seen by an outside observer, and $m(r)$ is the mass function defined by

$$m(r) = 4\pi \int_0^r \rho(\bar{r})\bar{r}^2 \mathrm{d}\bar{r}, \tag{8}$$

and $p(r)$, and $\rho(r)$ are respectively the pressure and density of the perfect fluid used to model the fluid interior. Furthermore requiring the regularity of the mass function, that is the mass function vanishes at the $r = 0$ coordinate from physical considerations: $m(r = 0) = 0$, fixes the value of the integration constants uniquely.

Enforcing the boundary conditions ensures the matching of the value of the metric coefficients at the boundary as is shown in Figure 1, leading to matching to a

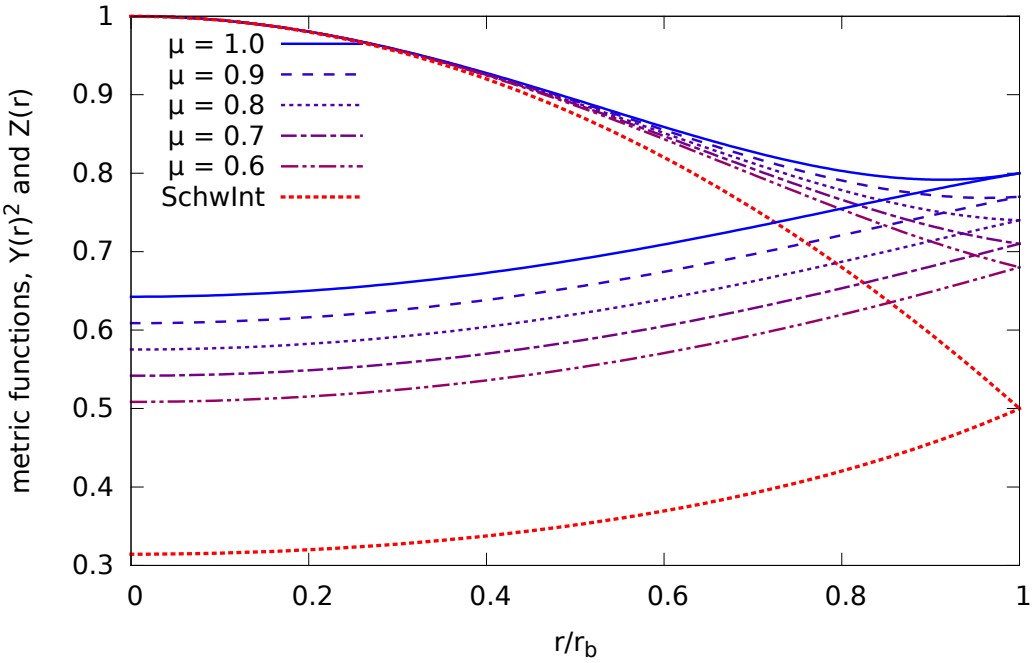

Figure 1: (Colour online) The Z and Y^2 metric functions with the radial coordinate inside the star for the TVII solution. The $Z(r)$ functions can be identified by the fact that $Z(r = 0) = 1$, for all μ. The parameter values are $\rho_c = 3/(16\pi)$ and μ taking the various values shown in the legend. Also shown for comparison is the Schwarzschild interior solution's metric functions abiding by the same boundary conditions. Visually the trend of $\lim_{\mu\to 0}(\mathrm{TVII}) \to \mathrm{SchwInt}$ is clear.

Schwarzschild exterior metric which is also shown next in Figure 2(a) and in Figure 2(b). In all the figures the Schwarzschild Interior solution, which was generated with the same parameter values as the Tolman VII solution is also shown, in an attempt to show the similarities between them. Now that the boundary conditions have been enforced, and hence a full solution to the Einstein equations been obtained, one can

begin to investigate the geometrical structure of this solution. However this endeavour is made difficult by the presence of *three* different parameters that can be changed simultaneously: ρ_c, r_b, and μ. Each of these change the character of the interior solution and the EOS quite drastically. This effect on the latter was shown previously in [2], whereas in this manuscript, being mainly interested in the former aspects, we proceed by fixing the only parameters usually available (measured) for these astrophysical objects: the mass and the radius.

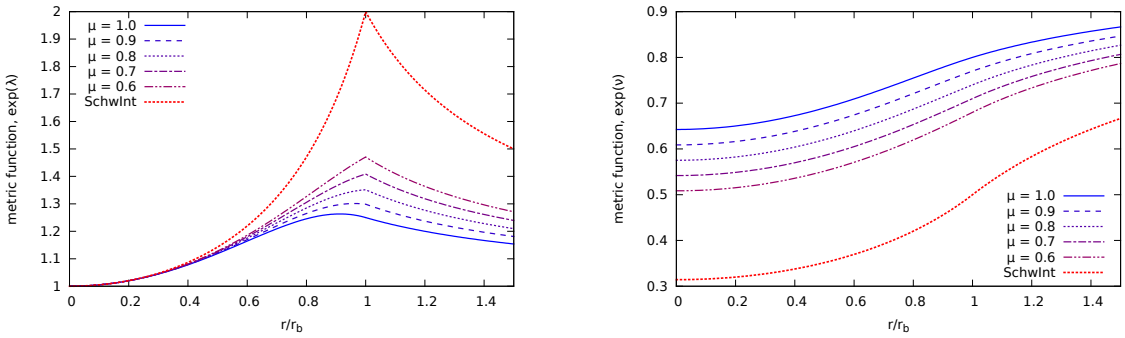

(a) The λ metric function

(b) The ν metric function

Figure 2: (Colour online) The metric functions with the radial coordinate inside and outside the star for the TVII solution. The parameter values are $\rho_c = 3/(16\pi)$ and μ taking the various values shown in the legend. The Schwarzschild interior metric for the same parameter values are also shown for comparison. Again the unmistakable trend of $\lim_{\mu\to 0}$ of TVII resulting in Schwarzschild interior is clear. The masses associated with these solutions are all different.

3. Mass in general relativity

In what follows, the Tolman VII solution is compared and contrasted to the Schwarzschild interior solution. In order to simplify the analysis, certain parameters will be fixed while others will be allowed to vary. The parameter that was kept fixed in the following is the external mass perceived at infinity: the mass that is used in the externally matched Schwarzschild exterior solution: typically $M = 1/4$ was used in all the figures. Through the use of geometric units, the higher Buchdahl [11] limit of $M = 4/9$, can be used directly(without unit conversions) and thus the use of $M = 1/4$ throughout gives some leeway in changing other parameters, while skirting around possible singular behaviour in the metric function.

This choice does not fix the solution uniquely, and in what follows either (i) the radius is fixed to some specific normalized value: typically to $r_b = 1$, and in so doing one varies the central densityρ_c to achieve the same external mass, or (ii) the central density is fixed to $\rho_c = 3/(16\pi)$ and the radius r_b of the sphere varied, while still

keeping the mass fixed. The one radius that is fixed for comparison purposes is the outer boundary of the Schwarzschild interior solution which is set to unity, in this case too. In either case, the dimensionless parameter μ, is varied to give comparisons to the Schwarzschild interior solution. As a result the following trends are expected to be visible: (i) since the mass is fixed, and the central density is changing while the radius is fixed, all discontinuities, if they exist, occur at $r_b = 1$ in the first set of figures **(a)**. Decreasing μ from one to zero then results in the central density decreasing so that one still gets a fixed mass while the boundary density can increase at $r_b = 1$. (ii) In the second set of figures **(b)**, decreasing μ from one to zero, increases the boundary radius r_b as is evident by the increasing r–coordinate of the discontinuities of the corresponding curves shown. We now give a brief description of the different masses appearing in the literature, to be able to distinguish between the Schwarzschild mass $M = m(r_b)$, the Tolman–Whittaker mass M_T and the proper mass M_P. The mass given in equation (8) is known as the Schwarzschild mass. This mass depends on the density ρ of the material source and does not take into account the gravitational energy. The usual method of including gravitational energy is through what is known as the Tolman–Whittaker(TW)–mass [12, 13] given by

$$M_T \coloneqq \int_V \left(T_0{}^0 - T_1{}^1 - T_2{}^2 - T_3{}^3\right)\sqrt{-g}\mathrm{d}V = 4\pi \int_0^{r_b} (\rho + 3p)\,\frac{r^2 Y}{\sqrt{Z}}\mathrm{d}r, \tag{9}$$

where $T_a{}^b$ are the components of the energy momentum tensor, and g is the metric determinant. The method of finding this expression involves the use of the Tolman pseudo-tensor density of gravitational energy t_a^b, is quite lengthy, and will not be given in full here, instead the reader is referred to [12, pg. 224] where full derivations of this quantity is provided.

This quantity is different from the proper mass M_P, which is also an integral over the proper space volume [14], but only on the energy density $T_0{}^0$, that is,

$$M_P \coloneqq \int_V \left(T_0{}^0\right)\sqrt{-g}\mathrm{d}V = \int_V \rho(r)\sqrt{-g}\mathrm{d}V, \tag{10}$$

and is commonly used in the TOV methods' point of view where it is compared to the total baryon rest mass. The difference between these latter two masses yields the "gravitational energy" of the star. However this terminology will not be used in this article since the main interest here is in the geometry of the solutions. Both the Schwarzschild and Tolman-Whittaker masses for these models are calculated, and the former mass is fixed to a value of $M = 1/4$ when appropriate, however just to provide an idea of the relative magnitudes of the three different masses and the effect of the parameter μ on them, Figure 3 is given.

The reason the Schwarzschild mass is fixed instead of the TW-mass is practical: it is easier to compute. Furthermore, the Buchdahl limit is usually expressed very succinctly in terms of the Schwarzschild mass which is also the mass that is measured at infinity by observers: and hence one can use observed values of masses of neutron stars as a guide in setting right magnitudes more easily.

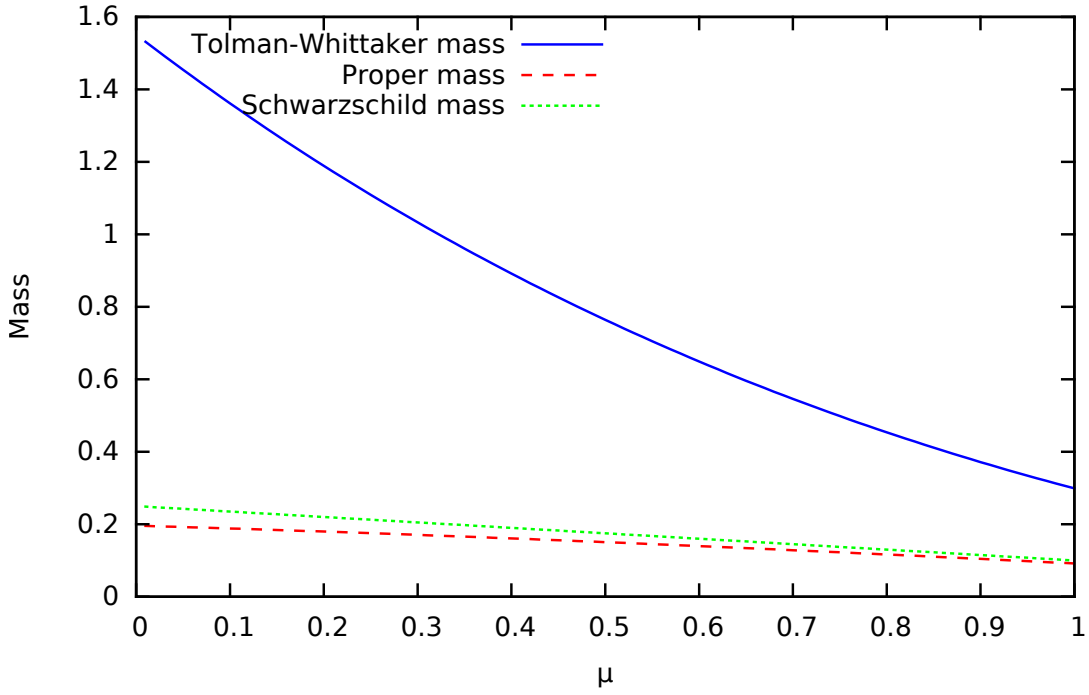

Figure 3: (Colour online) The 3 different masses with changing value of μ. Of importance is the much higher value of the Tolman–Whittaker mass, since it includes all the gravitational energy of the system. The difference between the Schwarzschild and proper mass is not very large, and is due to the appearance of the metric determinant in the latter integral.

4. The metric and geometrical structure

To proceed, first everything is re-expressed in terms of the mass as seen from an external point of view, since this is the only observable usually available to astronomers. By fixing this external mass, the external Schwarzschild metric is also fixed, and thus all the different coloured lines on the right of Figure 2a and Figure 2b will collapse into one single line, corresponding to the specified mass. The internal geometrical tensors however will be very different, while still giving the same external field. This rich structure will be made clear in the graphs presented, however first one re-expresses two of the three parameters, ρ_c, in terms of the mass through:

$$\rho_c = \frac{15M}{4\pi r_b^3(5-3\mu)}, \tag{11}$$

and similarly r_b:

$$r_b = \sqrt[3]{\frac{15M}{4\pi\rho_c(5-3\mu)}}, \tag{12}$$

where M is the Schwarzschild mass being fixed. Equations (11) and (12) will allow the investigation of the geometrical tensors inside the sphere whilst keeping the mass

constant, and still allow the flexibility of spanning the whole solution space from "natural" Tolman VII where $\mu = 1$ through "self-bound" Tolman VII when $0 < \mu < 1$, to finally Schwarzschild interior when $\mu = 0$.

In most of the plots, the boundary radius has been normalized at $r_b = 1$ for the Schwarzschild interior solution. When the boundary r_b of Tolman VII is actually varied, the different μ values together with the constant $\rho_c = 3/(16\pi)$ will achieve the same mass in the solutions. However when r_b is kept fixed at $r_b = 1$, the same exterior mass is obtained through changing ρ_c. In this article the causality condition which is an additional constraint that can be imposed on the solution after the functional form has been obtained will not be investigated. As a result some chosen parameter values might result in causality violations in the solution, however causality can be imposed if it were so desired. (See e.g. [2] for restrictions imposed by causality).

When the parameters are fixed as mentioned, one can look at the geometric tensors inside the sphere. First the metric functions e^{λ} and e^{ν} are investigated when the boundary radius in figure 4 is changing.

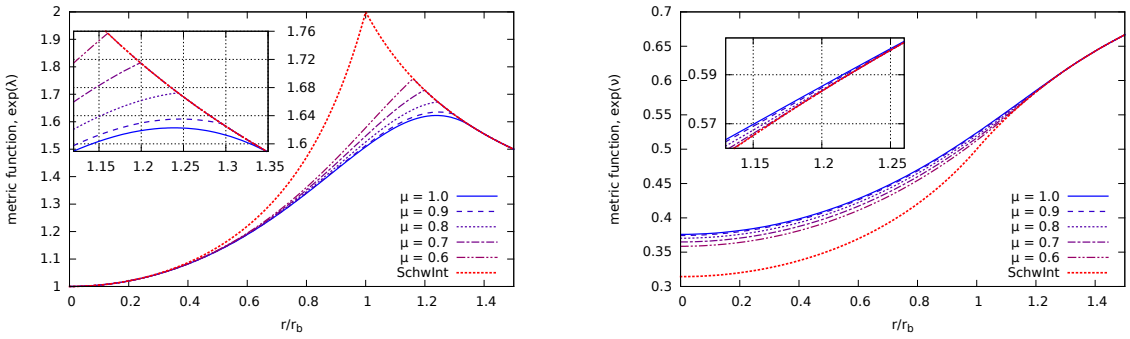

(a) The λ metric function

(b) The ν metric function

Figure 4: (Colour online) The metric functions with the radial coordinate inside and outside the star for the TVII solution. The parameter values are $M = 1/4, \rho_c = 3/(16\pi)$ and μ taking the various values shown in the legend. Also shown for comparison, the Schwarzschild interior metric for the same parameter values. Again the unmistakable trend of $\lim_{\mu\to 0}$ of TVII resulting in Schwarzschild interior is clear. The boundary radii associated with these solutions are all different.

In Figure 4(a) the normalization of the Schwarzschild interior at $r_b = 1$ is clearly seen. The same is true in Figure 4(b), but this particular feature is harder to see clearly. All the internal solutions match to the same exterior Schwarzschild metric by construction, even though they all do so at different radii. This is to be expected, with the $\mu = 1$ case having the maximum radius of $r_b = \sqrt[3]{5/2} \approx 1.36$, since the density shows the greatest transition (from a central value until it vanishes at the boundary), and to achieve the same mass with a smoother decrease in density a larger sphere is needed. The later case is also the only one where the matching of the metric function

results in the matching of the metric derivatives too: this is seen as the slope matching in those particular curves, at the point of contact between interior and exterior.

If instead one fixes $r_b = 1$ and varies the central density to achieve the same external mass, Figure 5 is obtained, and again one sees a similar pattern as the previous graph sets, with the smooth transition of the metric again occurring for the $\mu = 1$ curve only.

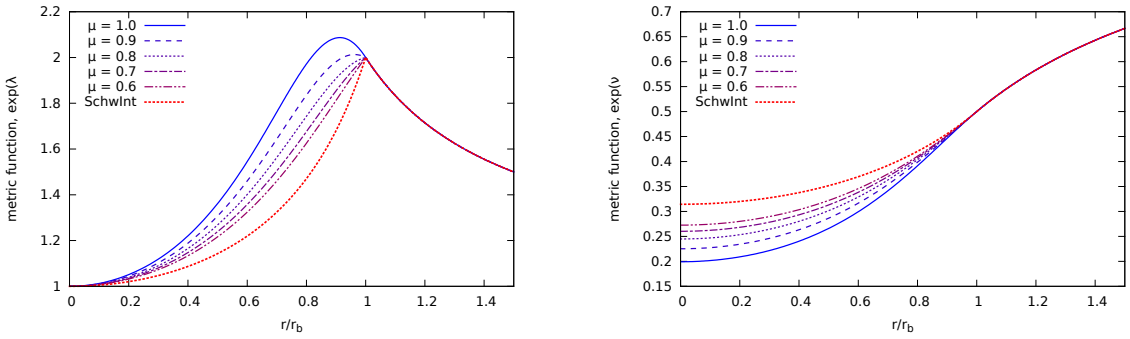

(a) The λ metric function

(b) The ν metric function

Figure 5: (Colour online) The metric functions with the radial coordinate inside and outside the star for the TVII solution. The parameter values are $M = 1/4$ and μ taking the various values shown in the legend. Also shown for comparison, the Schwarzschild interior metric for the same parameter values. Again the unmistakable trend of $\lim_{\mu\to 0}$ of TVII resulting in Schwarzschild interior is clear. The central density ρ_c associated with these solutions are all different.

From these metric functions, all other geometric tensors can be computed. However the interpretation of the Riemann tensor's components directly is difficult since many of the symmetries in this particular tensor make for multiple components to carrying the same information. Instead of analyzing the Riemann tensor R_{abcd} components directly, we will use its decomposition into its Weyl C_{abcd}, Ricci tensor $R_{ab} = g^{cd}R_{cadb}$, and Ricci scalar $R = g^{ab}R_{ab}$ contributions through

$$R_{abcd} = C_{abcd} - g_{a[d}R_{c]b} - g_{b[c}R_{d]a} - \frac{1}{3}Rg_{a[c}g_{d]b}, \tag{13}$$

to give a clearer picture of how these encode gravity together. It will be evident from these figures that the diagonal components of the Ricci tensor are non-zero inside the sphere, but must vanish in the Ricci-flat exterior at the star's boundary.

4.1. Ricci tensor components

While the central value of this Ricci component does not change by much in the first panel of Figure 6(a) which plots the Ricci tensor component R_{tt}, when μ gets progressively closer to zero, the discontinuity at the boundary does increase, the

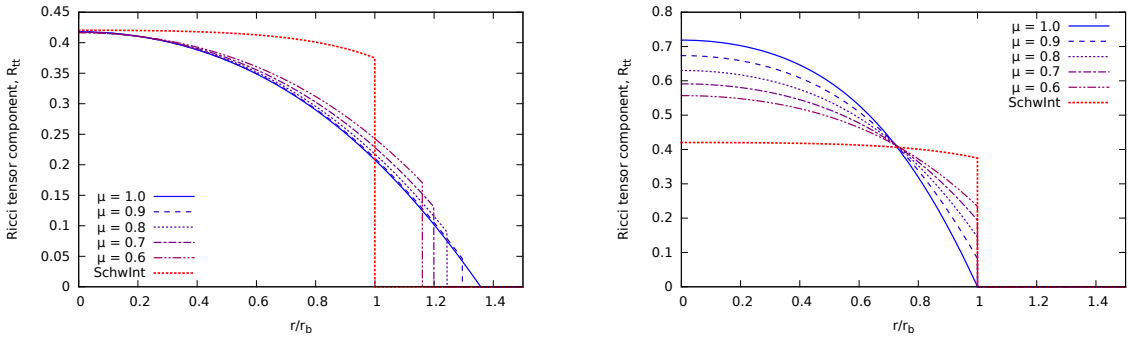

(a) Constant central density **(b)** Constant radius

Figure 6: (Colour online) The R_{tt} tensor component with the radial coordinate inside and outside the star for the TVII solution. The parameter values are $M = 1/4, \rho_c = 3/(16\pi)$ and μ taking the various values shown in the legend for figure (a), and $M = 1/4$ for figure (b). Also shown for comparison, the Schwarzschild interior metric for the same parameter values.

continuous curve being the one with $\mu = 1$: the "natural" case again. This trend is again seen in Figure 6(b), however with the central value changing too. The unmistakable trend of $\lim_{\mu\to 0}$ of TVII resulting in the Schwarzschild interior is clear.

The second Ricci tensor component: R_{rr} is shown next in Figure 7, where similar features are seen. The largest discontinuity occurs in the Schwarzschild interior case. The striking convergence of the curves at around $r \approx 0.839$ in the second panel Figure 7(b) is due to a lack of higher resolution that would show that the curves indeed cross at different points. However the value of R_{rr} in the exterior $r \geq r_b$ is identically zero.

Next the $R_{\theta\theta}$ component is shown in Figure 8. The unusual feature here is the completely different shape of the Schwarzschild interior component of the Ricci tensor. However an intuitive explanation of this feature is that since the Weyl tensor components which are shown next in Figures 10, 11, and 12 have to be zero in the Schwarzschild interior solution, the Ricci components have to compensate by having larger values so that the Riemann tensor inside is still non-zero. The convergence of the lines around $r \approx 0.8$ is again an effect of the lower resolution used in Figure 8(b)

The last diagonal Ricci component $R_{\varphi\varphi}$ is the same as $R_{\theta\theta}$ modulo a $\sin(\theta)$ term, and will not be shown here, instead the Ricci scalar: the trace of the Ricci tensor, is shown in Figure 9.

4.2. Weyl tensor components

Next all the non-zero Weyl tensor components are investigated. While there are six non-zero components, only three are unique. The first one of interest is the C_{trtr} component shown in Figure 10. The $C_{r\theta r\theta}$ and the $C_{r\varphi r\varphi}$ tensor components are the same as C_{trtr},

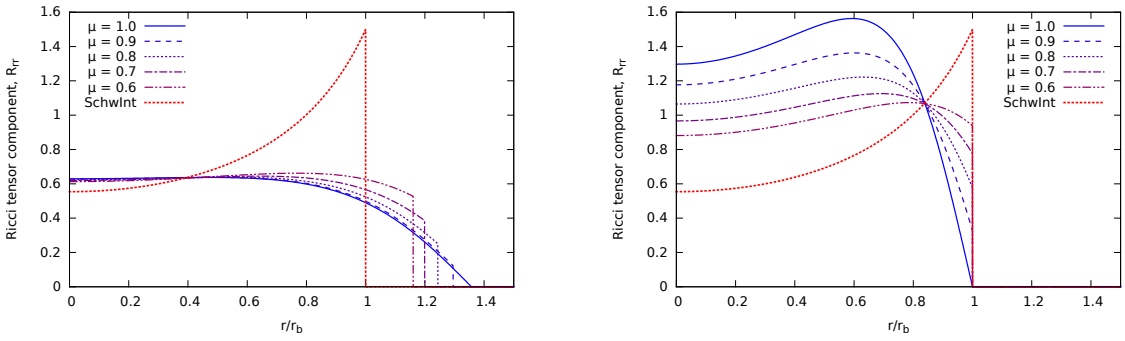

(a) Constant central density **(b)** Constant radius

Figure 7: (Colour online) The R_{rr} tensor component with the radial coordinate inside and outside the star for the TVII solution. The parameter values are $M = 1/4, \rho_c = 3/(16\pi)$ and μ taking the various values shown in the legend for figure(a), and $M = 1/4$ for figure (b). Also shown for comparison is the Schwarzschild interior metric for the same parameter values.

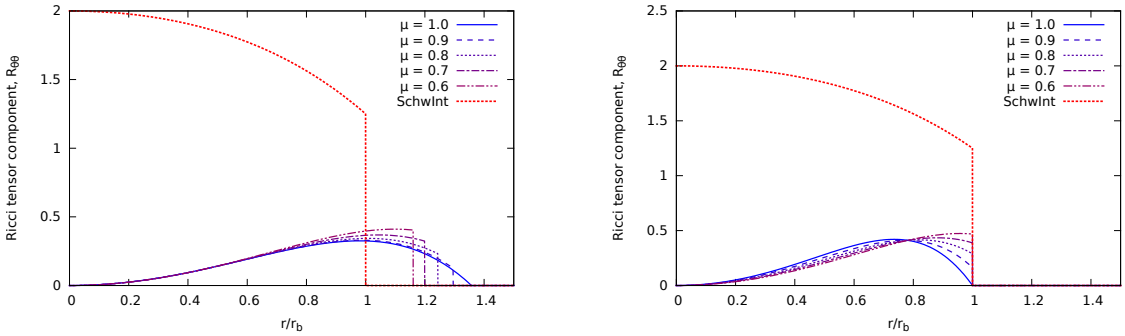

(a) Constant central density **(b)** Constant radius

Figure 8: (Colour online) The $R_{\theta\theta}$ tensor component with the radial coordinate inside and outside the star for the TVII solution. The parameter values are $M = 1/4, \rho_c = 3/(16\pi)$ and μ taking the various values shown in the legend for figure (a), and $M = 1/4$ for figure (b). Also shown for comparison is the Schwarzschild interior metric for the same parameter values.

and will not be shown separately. The Weyl tensor components can be understood in a similar way as the Ricci components. First one notes the same trend as noted previously; namely the continuity of the components in the natural ($\mu = 1$) case across the fluid boundary. The discontinuities become more and more pronounced as μ tends towards zero, with the largest discontinuity occurring in the Schwarzschild interior case, which is the formal $\mu \to 0$ limit. This trend is also clear in the constant radius case in Figure 10(b). Contrary to the Ricci case however, since the Schwarzschild *exterior*

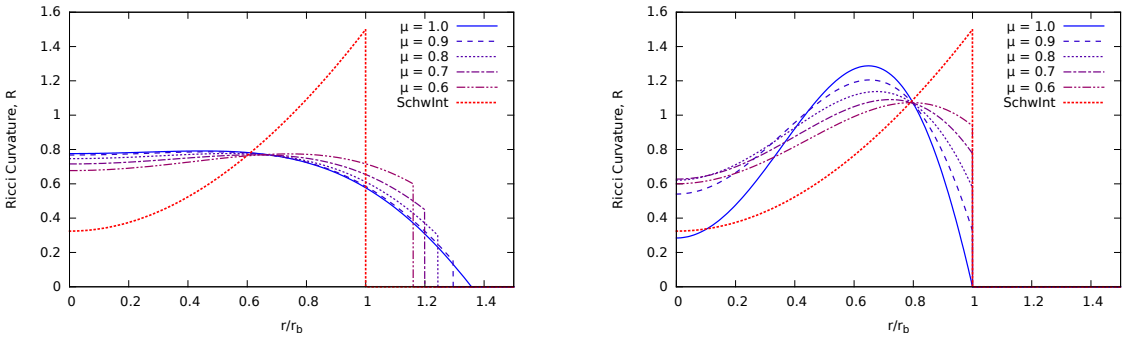

(a) Constant central density **(b)** Constant radius

Figure 9: (Colour online) The R scalar with the radial coordinate inside and outside the star for the TVII solution. The parameter values are $M = 1/4, \rho_c = 3/(16\pi)$ and μ taking the various values shown in the legend for figure (a), and $M = 1/4$ for figure (b). Also shown for comparison, the Schwarzschild interior metric for the same parameter values. The relationship between Tolman VII and Schwarzschild interior is clear in the constant density case, but much harder to see in the constant radius case.

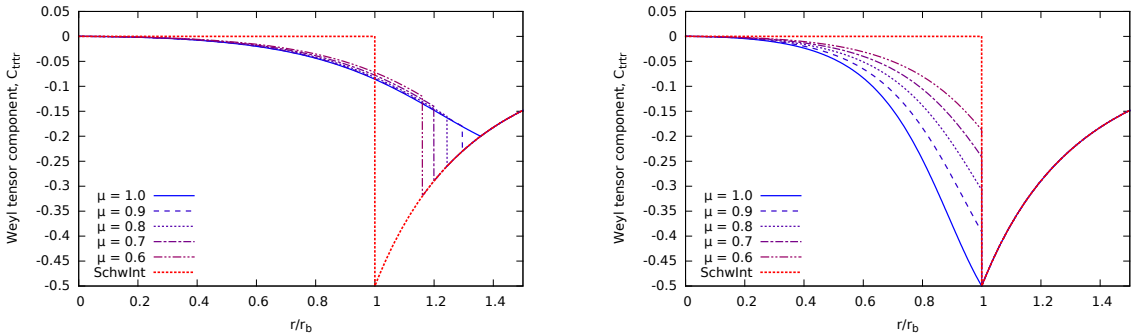

(a) Constant central density **(b)** Constant radius

Figure 10: (Colour online) The C_{trtr} tensor component with the radial coordinate inside and outside the star for the TVII solution. The parameter values are $M = 1/4, \rho_c = 3/(16\pi)$ and μ taking the various values shown in the legend for figure (a), and $M = 1/4$ for figure (b). Also shown for comparison is the Schwarzschild interior metric for the same parameter values.

solution is a pure Weyl solution, the tensor components do not vanish in the exterior, and one can see the $-2M/r^3$ fall off clearly. Furthermore the fact the the Schwarzschild interior is a pure Ricci solution becomes clear: The Weyl tensor components for this particular solution is identically zero everywhere inside the star.

Next the $C_{t\theta t\theta}$ component is shown in Figure 11. The main trends seen previously are still present in these, and the only drastically different behaviour is the slower fall

off of the Weyl tensor component as compared to the previous one in the exterior. This follows from the more complicated expression of that components which falls off as $1/r$ for large r in this case. The $C_{t\varphi t\varphi}$ behaviour is the same as that for $C_{t\theta t\theta}$, and is not shown separately.

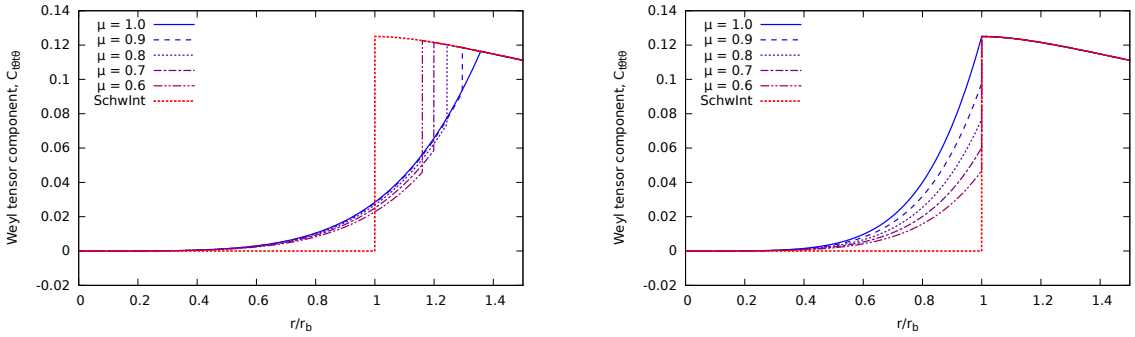

(a) Constant central density **(b)** Constant radius

Figure 11: (Colour online) The $C_{t\theta t\theta}$ tensor component with the radial coordinate inside and outside the star for the TVII solution. The parameter values are $M = 1/4, \rho_c = 3/(16\pi)$ and μ taking the various values shown in the legend for figure (a), and $M = 1/4$ for figure (b). Also shown for comparison is the Schwarzschild interior metric for the same parameter values.

The $C_{\theta\varphi\theta\varphi}$ component however is different and is shown in Figure 12. The increasing

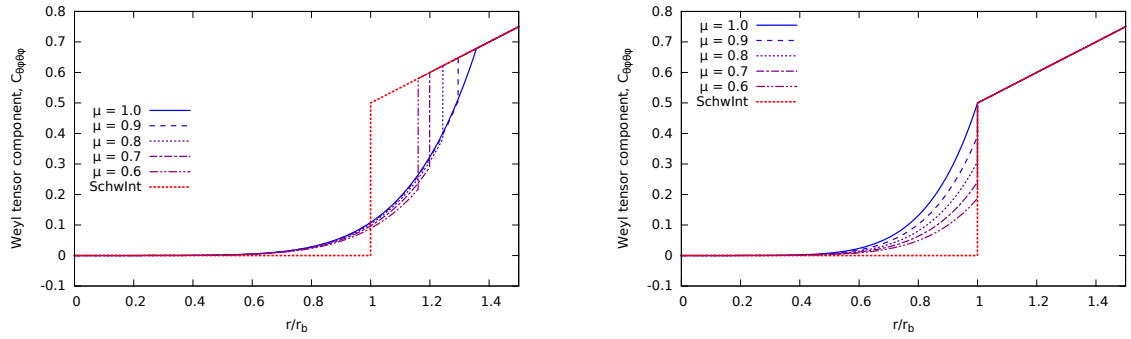

(a) Constant central density **(b)** Constant radius

Figure 12: (Colour online) The $C_{\theta\varphi\theta\varphi}$ tensor component with the radial coordinate inside and outside the star for the TVII solution. The parameter values are $M = 1/4, \rho_c = 3/(16\pi)$ and μ taking the various values shown in the legend for figure (a), and $M = 1/4$ for figure (b). Also shown for comparison is the Schwarzschild interior metric for the same parameter values.

Weyl tensor component in the exterior is surprising, as it would be expected that the

Weyl tensor should vanish at infinity. However this is only an artifact of using the fully covariant tensor *components* instead of $C^a{}_{bcd}$, which is more readily interpreted in a physical context: indeed, the latter form of the tensor components show no such increase to infinity for $r \to \infty$. The fully covariant components were used in this article because they made subsequent calculations simpler.

This ends the presentation of the Weyl tensor components. All of them show the same general trends relating the μ values from the Tolman VII solution to the Schwarzschild solution. The continuity of the $\mu = 1$, "natural" case is also readily apparent, and the larger discontinuities in the tensor components with decreasing μ up to the limiting Schwarzschild interior solution which needs zero interior Weyl component, but non-zero exterior values is seen in all the non identically zero components.

5. Tetrad formalisms

Another equivalent way of looking at the tensor components, but in a coordinate invariant way is through the use of the tetrad formalisms such as the Newman-Penrose (NP) formalism which uses a set of four null vectors to form a frame (vierbein), or the any other non-unique orthonormal set of four vectors to form the frame. Both methods will be investigated next, while keeping in mind that these are but different ways of looking at the same solution. The advantage of a tetrad formulation is that it provides definitions of a number of scalars. The scalars encode the same information as the tensor components investigated in the previous sections, without using the Einstein summation convention, while at the same time allowing the study of asymptotic behaviour of the curvature quantities [15].

5.1. An orthogonal tetrad

One proceeds by picking a frame through the definition of four orthonormal basis vectors

$$\boldsymbol{e}_{(0)}{}^a = \boldsymbol{v}^a = \left(\frac{1}{c_1 \cos(\phi\xi) + c_2 \sin(\phi\xi)}, 0, 0, 0 \right) \tag{14a}$$

$$\boldsymbol{e}_{(1)}{}^a = \boldsymbol{i}^a = \left(0, -\sqrt{ar^4 - br^2 + 1}, 0, 0 \right) \tag{14b}$$

$$\boldsymbol{e}_{(2)}{}^a = \boldsymbol{j}^a = \left(0, 0, -\frac{1}{r}, 0 \right) \tag{14c}$$

$$\boldsymbol{e}_{(3)}{}^a = \boldsymbol{k}^a = \left(0, 0, 0, -\frac{1}{r \sin\theta} \right) \tag{14d}$$

to define the orthonormal tetrad which will later be used to define a null tetrad for the NP-formalism. It should be mentioned that the notation for the different vectors and scalars calculated from them differ in most books, and here the notation used in the differential geometry package of Maple™ is what is being followed. The notation used in [15] and in [16] write R_{ab} for $R_{(a)(b)}$ so that $R_{(1)(1)}$ becomes R_{11} for example, and this can lead to confusion.

5.2. The NP tetrad

In the NP formalism, The null tetrad used in the usual notation are

$$\boldsymbol{e}_{(0)}{}^{a} = \boldsymbol{l}^{a} = \frac{1}{\sqrt{2}}\left(\frac{1}{c_1\cos(\phi\xi)+c_2\sin(\phi\xi)}, -\sqrt{ar^4-br^2+1}, 0, 0\right) \tag{15a}$$

$$\boldsymbol{e}_{(1)}{}^{a} = \boldsymbol{n}^{a} = \frac{1}{\sqrt{2}}\left(\frac{1}{c_1\cos(\phi\xi)+c_2\sin(\phi\xi)}, \sqrt{ar^4-br^2+1}, 0, 0\right) \tag{15b}$$

$$\boldsymbol{e}_{(2)}{}^{a} = \boldsymbol{m}^{a} = \frac{1}{\sqrt{2}}\left(0, 0, -\frac{1}{r}, -\frac{i}{r\sin\theta}\right) \tag{15c}$$

$$\boldsymbol{e}_{(3)}{}^{a} = \bar{\boldsymbol{m}}^{a} = \frac{1}{\sqrt{2}}\left(0, 0, -\frac{1}{r}, \frac{i}{r\sin\theta}\right) \tag{15d}$$

Where c_1, c_2, ϕ, ξ, a, and b have been given previously in equations (6a), (2), (3), and (5). This null tetrad can easily be obtained from the orthonormal basis above (14) through a well defined algorithm. From this null tetrad the spin coefficients and scalars can be calculated and plotted for this particular solution. Being in the static and spherically symmetric regime, the only Weyl scalar that does not vanish in this formalism will be Ψ_2, and the some of the Ricci scalars and rotation coefficients will also vanish because of the symmetry. Expressions and graphs of the non-vanishing scalars will be given in the appendix, and here only a few attributes of these scalars will be discussed.

The Ricci Scalars Φ_{00} and Φ_{11}, are related very simply through $\Phi_{00} = 2\Phi_{11}$, because of the isotropic nature of the energy-momentum tensor of this solution. Similarly the static and spherically symmetric nature of the solution manifests itself in the vanishing of all the Weyl scalars except for Ψ_2. It should therefore come to no surprise that Ψ_2, as the only Weyl scalar component, is related to Ponce de Leon's Weyl function W, introduced later in equation (16). Most of the spin coefficients vanish, and according to [15], the vanishing of κ^{NP}, a condition present in this solution, implies that the integral curve (congruence) of $\boldsymbol{l}_a = g_{ab}\boldsymbol{l}^a$, is a geodesic. From the expression of $\boldsymbol{l}^a$ in (15), and the form of the metric, this can be easily ascertained. Furthermore $\sigma^{\mathrm{NP}} = 0$, means that the congruence does not undergo any shear with increasing r, and ρ^{NP} being non-zero suggests that the congruence expands with increasing r. [17]

6. Discussion

The effects of having a non-zero density at the boundary(which is an equivalent way of saying that $\mu \neq 1$,) and the relation of this effect on the Weyl tensor components had previously been discussed in [18] and [1]. Of particular note is the fact that all the Weyl tensor components are related to a scalar function called W in [18], and which is defined through

$$W(r) = \frac{r^2Z'(Y-rY') + 2rZ(rY'-Y-r^2Y'') + 2rY}{12Y} \xrightarrow{\text{Tolman VII}} \frac{\kappa\mu\rho_c}{15r_b^2}r^5, \tag{16}$$

in the notation of this article. The last expression makes it clear that the value of $W(r_b)$ depends crucially on the value of μ, and indeed on the other parameters too. As a result

the dependence on μ is becomes clear that in the Schwarzschild interior solution, where μ is zero, W is zero too.

Ponce de Leon [18] also expressed the total mass inside the star as a function of W above as

$$m(r) = \frac{4\pi\rho_c r^3}{3} + W(r). \tag{17}$$

This equation can be interpreted in two ways: (i) with the Tolman VII solution seen as a generalization of the Schwarzschild interior solution, this relation suggests that the external perceived Schwarzschild mass is the exact same as the mass due to a sphere of *constant* density, where the central density of the Tolman VII solution determines the Schwarzschild interior density. This contribution corresponds to the first right hand term in the mass. Additionally a correction factor that on increasing the value of μ adds more and more mass to the sphere by reducing the boundary density discontinuity, achieving zero boundary density at the maximum value of W, is present. (ii) However one could also interpret this relation as a definition of W, and seen in this light W is measuring the contribution to the "free" gravitational field, or the free gravitational energy to the externally observed mass $M = m(r_b)$. This interpretation is further motivated by the realization [18] that $W(r) = rC^{\phi}{}_{\theta\phi\theta}$, exactly the same form of equation as $m(r) = rR^{\phi}{}_{\theta\phi\theta}$, furthering the idea that some gravitational aspects of the field that is similar to mass is being encapsulated by W. The usefulness of W, being clear, plots of this function in the constant central densities, and constant boundary radii cases are given in Figure 13.

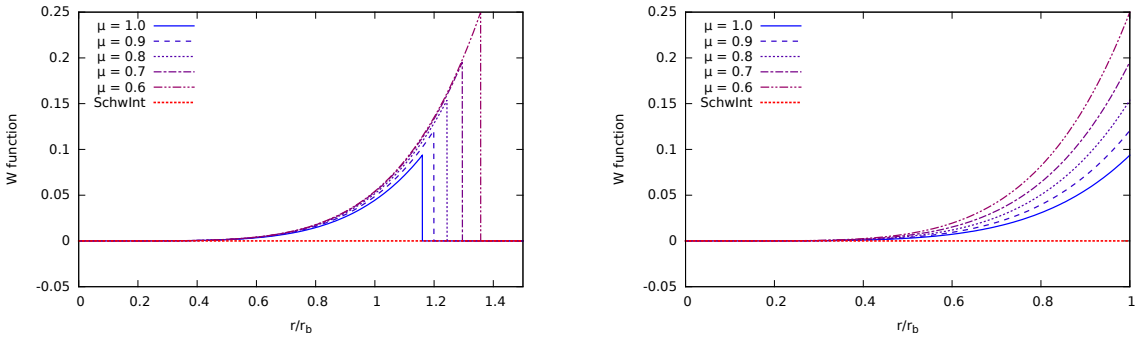

(a) Constant central density

(b) Constant radius

Figure 13: (Colour online) The W scalar function with the radial coordinate inside and outside the star for the TVII solution. The parameter values are $M = 1/4, \rho_c = 3/(16\pi)$ and μ taking the various values shown in the legend for figure (a), and $M = 1/4, r_b = 1$ for figure (b). Also shown for comparison is the Schwarzschild interior metric for the same parameter values.

It is immediately noticed that this function is always positive, and again according to [18], this is to be expected since W is only negative in cases where anisotropic

pressures exist: an issue that will be pursued in a later article. Furthermore, the Buchdahl limit of $M/r_b = 4/9$, cannot be exceeded with the Tolman VII solution for any parameter values, as exceeding this limit can only occur if $W < 0$. This concludes a geometrical overview of the Tolman VII solution.

Appendix A. NP-formalism scalars for the Tolman VII solution

All the NP spin coefficients are listed next. The standard notation according to [17, 13] is used throughout, but since some of the same symbols have already been used in the analysis of the Tolman VII solution, the NP coefficients are superscribed to differentiate them from the constants already used. First to the coefficients that vanish:

$$\lambda^{\rm NP} = \tau^{\rm NP} = \kappa^{\rm NP} = \sigma^{\rm NP} = \pi^{\rm NP} = \nu^{\rm NP} = 0. \tag{A.1}$$

The remaining non-vanishing ones which do not depend on either Y or Z are,

$$\beta^{\rm NP} = -\alpha^{\rm NP} = -\frac{\cot\theta}{2\sqrt{2}r}, \tag{A.2}$$

as expected from the spherical symmetry of this solution. These are the usual spherical coordinates spin coefficient, and they will not be analyzed any further.

The other spin coefficients which are in terms of the Z metric coefficient only are,

$$\mu^{\rm NP} = \rho^{\rm NP} = \frac{1}{r}\sqrt{\frac{\kappa\mu\rho_c r^4 - 5\kappa\rho_c r_b^2 r^2 + 15 r_b^2}{30 r_b^2}}, \tag{A.3}$$

and they are plotted next for clarity and completeness in Figure A1. Since there is an asymptote at $r = 0$, as is evident in the expression (A.3), the plots in Figure A1 show a "corrected" spin coefficient given by $r \times \mu^{\rm NP}$, so that the behaviour for small r can also be shown in the same figure. For $\mu = 1, \mu^{\rm NP}$ is continuous as is its radial derivative at $r = r_b$. Finally the remaining spin coefficients which consist of functions of both Y and Z are

$$\gamma^{\rm NP} = \epsilon^{\rm NP} = -\frac{1}{2}\sqrt{\frac{\kappa\mu\rho_c r^4 - 5\kappa\rho_c r_b^2 r^2 + 15 r_b^2}{30 r_b^2}} \left\{ \frac{\mathrm{d}}{\mathrm{d}r} \log\left[c_1 \cos(\phi\xi) + c_2 \sin(\phi\xi)\right] \right\}, \tag{A.4}$$

where all the constants used in the above have been specified before in terms of the three μ, ρ_c and r_b, and ξ has been used as an abbreviated form for $\xi(r)$ given in equation (5). The above $\gamma^{\rm NP}$ is shown in Figure A2.

Most of the the Weyl scalars vanish because of the spherically symmetric and static nature of the solution so that

$$\Psi_0^{\rm NP} = \Psi_1^{\rm NP} = \Psi_3^{\rm NP} = \Psi_4^{\rm NP} = 0, \tag{A.5}$$

except for $\Psi_2^{\rm NP}$, which simplifies considerably after a lot of algebra to the expression

$$\Psi_2^{\rm NP} = -\frac{\kappa\mu\rho_c}{15 r_b^2} r^2. \tag{A.6}$$

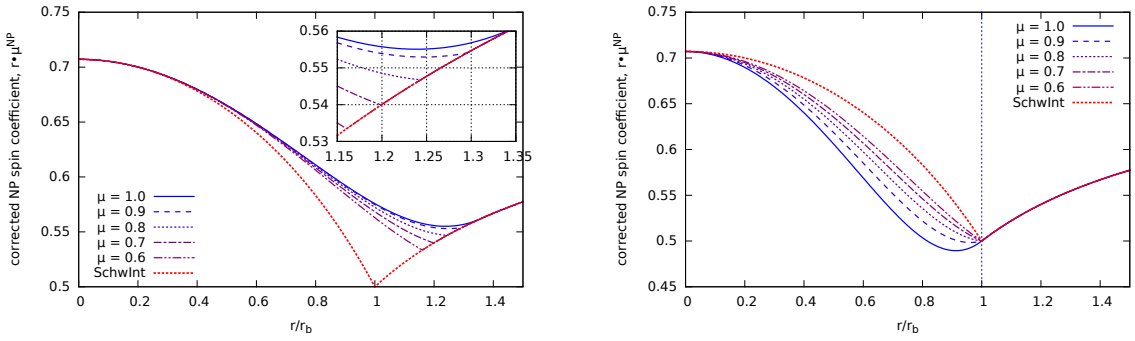

(a) Constant central density **(b)** Constant radius

Figure A1: (Colour online) The "corrected" μ^{NP} spin coefficient with the radial coordinate. The parameter values are $M = 1/4, \rho_c = 3/(16\pi)$ and μ taking the various values shown in the legend for figure (a), and $M = 1/4$ for figure (b). Also shown for comparison is the Schwarzschild interior metric for the same parameter values.

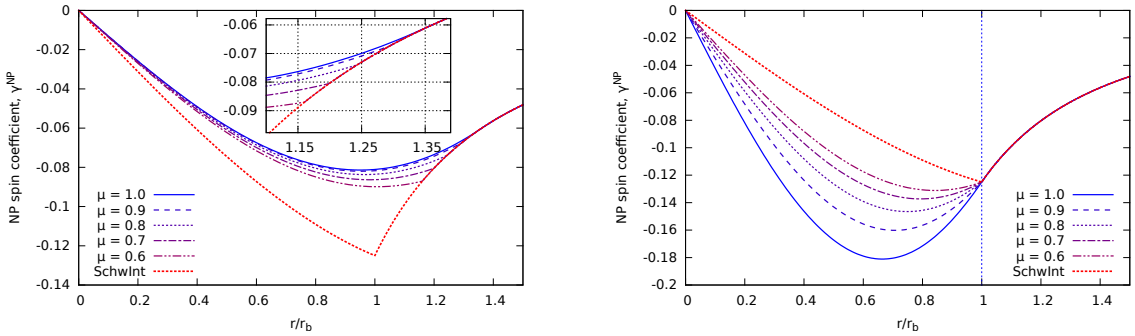

(a) Constant central density **(b)** Constant radius

Figure A2: (Colour online) The γ^{NP} spin coefficient with the radial coordinate. The parameter values are $M = 1/4, \rho_c = 3/(16\pi)$ and μ taking the various values shown in the legend for figure(a), and $M = 1/4$ for figure (b). Also shown for comparison is the Schwarzschild interior metric for the same parameter values.

This is very reminiscent of the function W which also simplified to the expression (16). One can conclude that indeed Ponce de Leon's function is related to the NP-Weyl scalar through the relation,

$$\Psi_2^{\mathrm{NP}} = -\frac{W}{r^3}. \tag{A.7}$$

This relation Ψ_2^{NP} will not be plotted and instead the reader is referred to Figure 13 for $W(r)$. The vanishing of most of the Weyl scalars (A.5) and Ψ_2 being non-zero also proves that Tolman VII is a solution of Petrov type D: It has two repeated principal null vectors: $\boldsymbol{l}_a$, and $\boldsymbol{n}_a$, expected from a static and spherically symmetric solution.

Continuing to look at the other scalar functions of the NP-formalism by turning to the Ricci scalar functions, one finds that some of them vanish identically:

$$\Phi_{01}^{\mathrm{NP}} = \Phi_{02}^{\mathrm{NP}} = \Phi_{12}^{\mathrm{NP}} = 0, \tag{A.8}$$

while the non-vanishing ones are given by

$$\Phi_{00}^{\mathrm{NP}} = \Phi_{22}^{\mathrm{NP}} = \frac{b}{2} - ar^2 + \frac{ar^4 - br^2 + 1}{2r}\left\{\frac{\mathrm{d}}{\mathrm{d}r}\left[\log\left(c_1\cos\left(\phi\xi\right) + c_2\sin\left(\phi\xi\right)\right)\right]\right\}, \tag{A.9}$$

and these are shown in Figure A3 and,

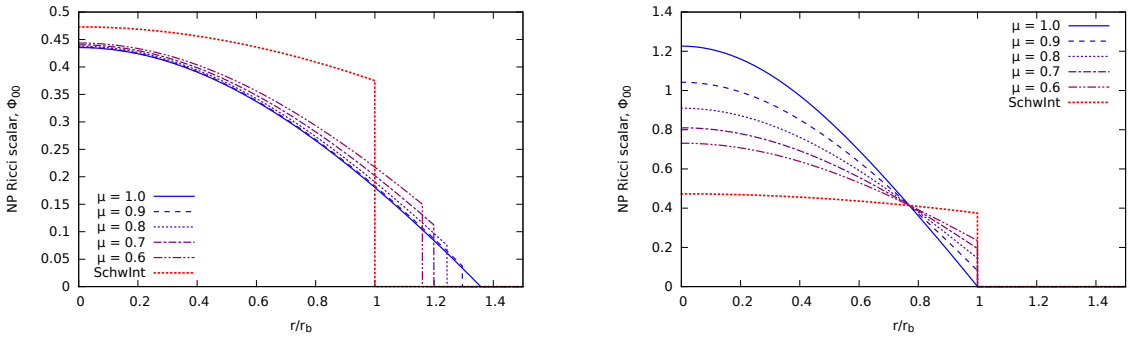

(a) Constant central density **(b)** Constant radius

Figure A3: (Colour online) The Φ_{00}^{NP} NP Ricci scalar with the radial coordinate. The parameter values are $M = 1/4, \rho_c = 3/(16\pi)$ and μ taking the various values shown in the legend for figure (a), and $M = 1/4$ for figure (b). Also shown for comparison is the Schwarzschild interior metric for the same parameter values.

$$\Phi_{11}^{\mathrm{NP}} = \frac{1}{4}\left\{b - ar^2 + \left[\frac{1 - br^2 + ar^4}{c_1\cos\left(\phi\xi\right) + c_2\sin\left(\phi\xi\right)}\right]\frac{\mathrm{d}^2}{\mathrm{d}r^2}(c_1\cos\left(\phi\xi\right) + c_2\sin\left(\phi\xi\right)) + \right.$$
$$\left. + \left(2ar^3 - br\right)\frac{\mathrm{d}}{\mathrm{d}r}\left[\log\left(c_1\cos\left(\phi\xi\right) + c_2\sin\left(\phi\xi\right)\right)\right]\right\}, \tag{A.10}$$

which is shown in Figure A4. The two graphs, and functions are related to each other by

$$\Phi_{11} = \frac{\Phi_{00}}{2}, \tag{A.11}$$

and this is a result that can be shown through the isotropy relation $G_r{}^r = G_\theta{}^\theta$. Using the latter, and substituting for the second derivative in (A.10) results in (A.11) The NP Ricci scalar which is related to the Ricci scalar is given by

$$\Lambda = \frac{1}{12}\left\{3b - 5ar^2 - \left[\frac{1 - br^2 + ar^4}{c_1\cos\left(\phi\xi\right) + c_2\sin\left(\phi\xi\right)}\right]\frac{\mathrm{d}^2}{\mathrm{d}r^2}[c_1\cos\left(\phi\xi\right) + c_2\sin\left(\phi\xi\right)] + \right.$$
$$\left. + \left[\frac{3br^2 - 4ar^4 - 2}{12r}\right]\frac{\mathrm{d}}{\mathrm{d}r}\left[\log\left(c_1\cos\left(\phi\xi\right) + c_2\sin\left(\phi\xi\right)\right)\right]\right\}, \tag{A.12}$$

and is shown in Figure A5. This completes the list of NP scalars and rotation coefficients.

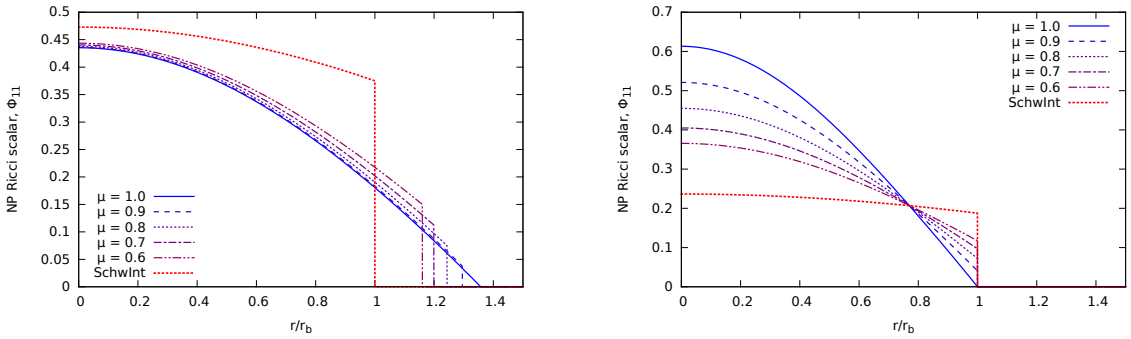

(a) Constant central density **(b)** Constant radius

Figure A4: (Colour online) The Φ_{11}^{NP} NP Ricci scalar with the radial coordinate. The parameter values are $M = 1/4, \rho_c = 3/(16\pi)$ and μ taking the various values shown in the legend for figure (a), and $M = 1/4$ for figure (b). Also shown for comparison is the Schwarzschild interior metric for the same parameter values.

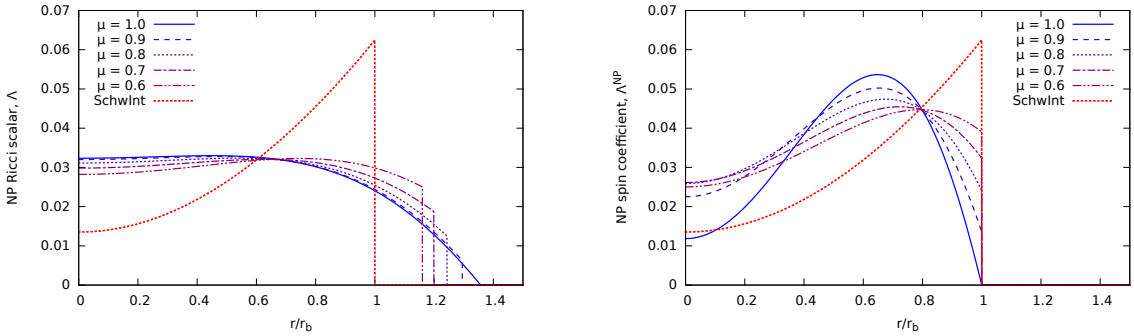

(a) Constant central density **(b)** Constant radius

Figure A5: (Colour online) The Λ^{NP} NP Ricci scalar with the radial coordinate. The parameter values are $M = 1/4, \rho_c = 3/(16\pi)$ and μ taking the various values shown in the legend for figure (a), and $M = 1/4$ for figure (b). Also shown for comparison is the Schwarzschild interior metric for the same parameter values.

[1] Raghoonundun A M 2009 *Properties of exact analytic models for neutron stars* Master's thesis University of Calgary
[2] Raghoonundun A M and Hobill D W 2015 *Phys. Rev. D* **92**(12) 124005 URL `http://link.aps.org/doi/10.1103/PhysRevD.92.124005`
[3] Tolman R C 1939 *Physical Review* **55** 364–373
[4] Delgaty M S R and Lake K 1998 *Computer Physics Communications* **115** 395–415
[5] Finch M R and Skea J E F 1998 A review of the relativistic static sphere unpublished, available at `www.dft.if.uerj.br/usuarios/JimSkea/papers/pfrev.ps`
[6] Ivanov B V 2002 *Physical Review D* **65** 104001
[7] Durgapal M C and Rawat P S 1980 *Mon. Not. R. Astron. Soc.* **192** 659–662
[8] Durgapal M C and Gehlot G L 1971 *Journal of Physics A: General Physics* **4** 749–755
[9] Neary N, Ishak M and Lake K 2001 *Physical Review D* **64** 084001
[10] Synge J 1960 *Relativity: the general theory* Series in physics (North-Holland Pub. Co.)
[11] Buchdahl H A 1959 *Phys. Rev.* **116**(4) 1027–1034
[12] Tolman R C 1966 *Relativity, Thermodynamics and Cosmology* The international series of monagraphs on physics (Clarendon press)
[13] Landau L and Lifshitz E 1980 *The Classical Theory of Fields* 4th ed (Butterworth-Heinemann)
[14] Haensel P, Potekin A and Yakovlev D 2007 *Neutron Stars 1 : Equation of State and Structure* vol 1 (Springer)
[15] Newman E and Tod K 1980 Asymptotically flat space-times *General Relativity and Gravitation: One Hundred Years After the Birth of Albert Einstein* vol 2 ed Held A (New York, U.S.A.: Plenum Press) pp 1–36
[16] Chandrasekhar S 1998 *The Mathematical Theory of Black Holes* Oxford classic texts in the physical sciences (Clarendon Press) ISBN 9780198503705
[17] Newman E and Penrose R 1962 *Journal of Mathematical Physics* **3** 566–578
[18] Ponce de Leon J 1988 *Phys. Rev. D* **37** 309–317